INTERNATIONAL JOURNAL FOR NUMERICAL METHODS IN FLUIDS
Int. J. Numer. Meth. Fluids 2008; **56**:167–184
Published online 22 May 2007 in Wiley InterScience (www.interscience.wiley.com). DOI: 10.1002/fld.1524

Side-wall effects on the bifurcation of the flow through a sudden expansion

Yeng-Yung Tsui*,† and Hong-Wen Wang

Department of Mechanical Engineering, National Chiao Tung University, Hsinchu 300, Taiwan, Republic of China

SUMMARY

Three-dimensional computations have been performed to study the flow through a symmetric sudden expansion with an expansion ratio of 3 at low Reynolds numbers. The aspect ratio of the flow channel is allowed to vary within a wide range to examine its influence on the flow which bifurcates from a symmetric state to an asymmetric state. The results reveal that the critical Reynolds number of the symmetry-breaking bifurcation increases while the aspect ratio is reduced. The flow behaviour near the side walls is illustrated by using limiting streamlines. The origin of the singular points identifiable on the side wall can be traced back to the recirculating flows and the relevant reattachment/separation points in the core of the channel. It is seen that the determination of the exact critical Reynolds number is not trivial because it depends on how to define asymmetric flow. Computations have also been conducted to show that a slight asymmetry in the channel geometry causes a smooth transition from symmetric to non-symmetric states. Copyright © 2007 John Wiley & Sons, Ltd.

Received 16 May 2006; Revised 5 April 2007; Accepted 7 April 2007

KEY WORDS: flow bifurcation; symmetry breaking; recirculating flows; side-wall effects

1. INTRODUCTION

The laminar flow through a sudden expansion in a channel will inevitably separate. For a symmetric, double-sided expansion two recirculation regions are formed behind the two expansion steps. It was shown in the experimental work of Durst *et al*. [1] that the flow is symmetric to the centreline of the channel at a Reynolds number of 56 (where the Reynolds number is based on the centreline velocity and the height of the channel), but becomes asymmetric as the Reynolds number is

*Correspondence to: Yeng-Yung Tsui, Department of Mechanical Engineering, National Chiao Tung University, Hsinchu 300, Taiwan, Republic of China.
†E-mail: yytsui@mail.nctu.edu.tw

Contract/grant sponsor: National Science Council of Republic of China; contract grant/numbers: NSC-91-2212-E-009-051 and NSC-93-2212-E-009-012

increased to 140, with two recirculation regions of unequal sizes. The formation of the asymmetric flow is sometimes attributed to the Coanda effect [2, 3]: once an increase (or decrease) in velocity at one wall is accompanied with a decrease (or increase) in pressure, the pressure difference formed across the channel will maintain the asymmetric pattern. The physical origin of the asymmetry is related to the instability of the shear layer between the main stream and the recirculating flow. Small disturbances embedded in the shear layer can be amplified to form wavy patterns and, then, vortex-like structures. Such a vortex-like shedding structure was detected in the double-sided sudden expansion flows studied by Cherdron *et al*. [4]. Due to the confinement of the channel the two shear layers on the two sides of the intake stream interact with each other through velocity fluctuations. If the fluctuating normal velocities in one shear layer are out of phase with those in the other, the vortex-like shedding flow becomes asymmetric [4]. The asymmetric flow patterns were captured in two-dimensional simulations by Tsui and Wang [5] and Tsui and Shu [6]. As pointed out by them, the asymmetric disturbances, required to trigger the asymmetric solution, can be generated either by the computer's round-off errors or by asymmetric relaxation methods used as matrix solvers.

The stability analyses of Fearn *et al*. [7] and Shapira *et al*. [8] showed that the unique, symmetric solution loses its stability at a certain critical Reynolds number beyond which a pair of stable, asymmetric solutions exists. This is referred to as supercritical pitchfork bifurcation. Because the symmetry-breaking point is structurally unstable, any type of small perturbation to the base flow problem, such as a slight degree of asymmetry in the expansion geometry as proposed by Fearn *et al*. [7], can lead to a breaking of the pitchfork bifurcation diagram into two branches. The primary branch describes a smooth transition from the symmetric solution to the asymmetric solution, whereas on the secondary branch there are two asymmetric solutions with one solution being stable and the other unstable [9, 10]. By further increasing the Reynolds number the flow may become three-dimensional before it becomes unsteady, as suggested by Fearn *et al*. [7]. An alternative is for the flow to evolve into a time-periodic state, which remains essentially two dimensional [3, 11, 12]. This is known as Hopf bifurcation. In a recent study the non-Newtonian fluid flow through a symmetric sudden expansion was investigated by Neofytou and Drikakis [13] using three models. Similar to the Newtonian flow, the breaking of the symmetric pattern also occurs at a critical point which depends upon the Reynolds number and the specific parameters included in each of the three models.

The methods adopted to find the critical Reynolds number for the pitchfork bifurcation can be classified into three categories: bifurcation analyses, numerical simulations and experiments. In the bifurcation analysis either stability analyses (linear or nonlinear) [8, 10, 14, 15] or extended system techniques [7, 16] were adopted to pinpoint the exact bifurcation point. For the other two methods it is required to gradually increase or decrease the Reynolds number to search for the critical point asymptotically. Besides, as mentioned above, the critical Reynolds number is sensitive to small imperfections that are unavoidable especially in the experimental apparatus. Therefore, it is rather difficult to exactly locate this point by these two methods.

A summary of reported critical Reynolds numbers obtained using the above methods for expansion ratios in the range 2–5 is listed in Table I. The Reynolds numbers shown in the table are based on the average inlet velocity and the intake channel height. It is evident that there is an inverse relationship between the critical Reynolds number and the expansion ratio. In general, the critical Reynolds numbers obtained by using various bifurcation analyses are close. For expansion ratio 2 they range from 143.6 to 145.3 while for expansion ratio 3 they fall in the range 53.3–55. The numerically predicted critical numbers are diversified. Among them only Drikakis [17] reported

DOI: 10.1002/fld

Table I. A summary of critical Reynolds numbers obtained by different methods.

H/h	Re_c	References	Methods
	143.7	Shapira *et al*. [8]	Bifurcation analysis
	145.3	Alleborn *et al*. [14]	Bifurcation analysis
	143.6	Battaglia *et al*. [16]	Bifurcation analysis
2	83.3	Durst *et al*. [11]	Numerical simulation
	150–155	Battaglia *et al*. [16]	Numerical simulation
	144	Drikakis [17]	Numerical simulation
	123.3	De Zilwa *et al*. [18]	Numerical simulation
	123.3	Chedron *et al*. [4]	Experiments
	53.9	Fearn *et al*. [7]	Bifurcation analysis
	55	Shapira *et al*. [8]	Bifurcation analysis
	53.3	Alleborn *et al*. [14]	Bifurcation analysis
	53.8	Battaglia *et al*. [16]	Bifurcation analysis
	53.8	Rusak and Hawa [15]	Bifurcation analysis
3	53.7	Mizushima and Shiotani [10]	Bifurcation analysis
	53.3	Foumeny *et al*. [19]	Numerical simulation
	57–58	Battaglia *et al*. [16]	Numerical simulation
	53.3	Drikakis [17]	Numerical simulation
	58.7	De Zilwa *et al*. [18]	Numerical simulation
	54.3	Schreck and Schafer [20]	Numerical simulation (three-dimensional)
	35.8	Battaglia *et al*. [16]	Bifurcation analysis
4	35–40	Battaglia *et al*. [16]	Numerical simulation
	35.3	Drikakis [17]	Numerical simulation
	28.5	Alleborn *et al*. [14]	Bifurcation analysis
5	28.4	Battaglia *et al*. [16]	Bifurcation analysis
	27–30	Battaglia *et al*. [16]	Numerical simulation
	27.3	Drikakis [17]	Numerical simulation

values in close agreement with those obtained from bifurcation analyses for the various expansion ratios. Either Foumeny *et al*. [19] or Schreck and Schafer [20] also obtained a critical value close to the theoretical values for expansion ratio 3. For expansion ratio 2 the critical value of 83.3 reported by Durst *et al*. [11] is not reliable because, comparing with the other data, it is far too low. The value of 123.3 predicted by De Zilwa *et al*. [18] is identical to the experimental data of Cherdron *et al*. [4], but about 14% lower than those obtained from bifurcation theory. Battaglia *et al*. [16] did not pinpoint exact values in their numerical simulations, but indicated an interval for each case. The interval is in the range 150–155 for expansion ratio 2 and in the range 57–58 for expansion ratio 3, which are on the side higher than the theoretical values.

In all the above studies, apart from that by Shreck and Schafer [20], the flow was assumed to be two dimensional. In the present study a three-dimensional numerical procedure is employed to investigate the effect of the side wall on the flow at Reynolds numbers around the bifurcation point. It was observed in both the experiments of Cherdron *et al*. [4] and the three-dimensional computations by Shreck and Schafer [20] that a decrease in the aspect ratio of the channel has a stabilizing effect which extends the range of Reynolds number for the symmetric flow to exist. A numerical investigation has been carried out by Chiang *et al*. [21] to examine the

DOI: 10.1002/fld

side-wall effect for a flow with expansion ratio of 3 and Reynolds number of 80 (based on the mean velocity and the channel height at the inlet). At this Reynolds number the flow is unavoidably asymmetric. However, the decrease of aspect ratio makes the flow undergo a transition towards symmetry. In addition to the bifurcation in the step height direction, the computations of Chiang *et al*. [22] revealed a symmetry breaking in the spanwise direction. In this kind of bifurcation the flow patterns are not symmetric, but skew symmetric to the mid-span plane; the two recirculation zones interchange their positions on the two sides of the mid-span plane. As indicated by them, it is rather difficult to obtain this spanwise bifurcation because symmetric flow is present on the mid-span plane, which is unstable according to the two-dimensional bifurcation theory. A recent study by Biswas *et al*. [23] showed some interesting results for the channel flow over a single-sided backward-facing step. For an expansion ratio of 1.9423 the reattached point behind the step is under-predicted in two-dimensional simulations for Reynolds numbers, Re, greater than 400 compared with experimental data (Re is based on the hydraulic diameter $D_h = 2h$, where h is the height of the intake channel). By conducting a three-dimensional calculation the separation line on the bottom wall is well captured. This reveals that to accurately simulate expansion flows at sufficiently large Reynolds numbers three-dimensional calculations become indispensable.

In this paper numerical simulations of the flow field are performed using a finite-volume method. A description of the flow configuration and the formulation of the problem are given in Section 2. This is followed by presentation of the numerical algorithm used to solve governing equations. The procedure is then tested and employed to examine the three-dimensional flow in the expansion channel. Finally, a concluding remark is made.

2. MATHEMATICAL MODEL

The physical model under consideration is illustrated in Figure 1. A channel with height H and length L_2 is preceded by a smaller channel with height h and length L_1. All computations are performed for an expansion ratio $H/h = 3$. The width of the two channels are denoted by W. The aspect ratio of the larger channel (W/H) will not be greater than 8 in most cases. All dimensions are

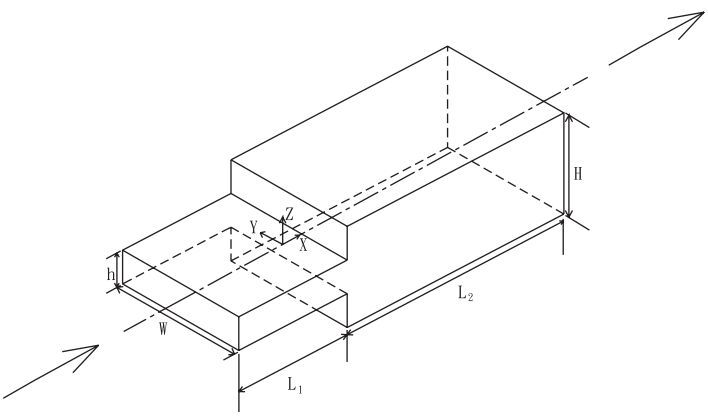

Figure 1. A schematic drawing of the expanded channel.

DOI: 10.1002/fld

scaled by using h as the reference length and the velocities are normalized by the bulk velocity in the upstream channel $\overline{U}$. The Reynolds number is defined as $Re = \overline{U}h/v$, where v is the kinematic viscosity. The governing equations to conserve mass and momentum for incompressible flow can then be cast into the following form:

$$\nabla \bullet \mathbf{V} = 0 \tag{1}$$

$$\nabla \bullet (\mathbf{VV}) = -\nabla P + \frac{1}{Re}\nabla^2 \mathbf{V} \tag{2}$$

Non-slip boundary conditions are imposed on the confining walls. At the inlet a uniform distribution of velocity is prescribed. Selection of the upstream channel length L_1 is made to ensure a fully developed state obtained before the flow entering the expanded channel. The length L_1 is $30h$ for most cases, but extended to $50h$ for aspect ratios W/h less than 3 at large Reynolds numbers in the range 150–200. It is known that for a fully developed duct flow with a square cross section (aspect ratio being one) the maximum velocity is twice the bulk velocity while for the two-dimensional channel flow the velocity ratio is 1.5. Hence, the flows with low aspect ratios require longer entrance length than those with large aspect ratios to reach fully developed state. Computations have shown that the lengths of the recirculation regions downstream of the sudden expansion will not exceed $20h$ in the present study. Thus, the use of $50h$ for the length L_2 is long enough for the flow to recover from the recirculating flows behind the step. At the exit the zero-gradient condition is imposed.

3. NUMERICAL METHOD

The governing equations are discretized using the finite-volume method, by which the equations are integrated over the control volume of a selected mesh first. The mesh is traditionally arranged in the structured manner in which each control volume is addressed through specifying indices i, j, and k. To deal with irregular geometry, one way is to construct the mesh using body-fitted curvilinear lines. In this method a transformation of the coordinate system must be entailed, resulting in emergence of a number of cross-derivatives and, thus, loss of strong conservation property of the original differential equations. The use of curvilinear grids solely cannot cope with very complicated geometry. To soothe this problem the zonal approach is sometimes incorporated. In this approach the flow field is divided into a number of blocks and each block is covered by a structured grid. Solution is sought in each block in a sequential fashion and iteration among the blocks must be carried out. Special care must be taken at the interface between neighbouring blocks to ensure coupling. An alternative, which can circumvent the above inconveniences, is the use of unstructured grids. In this approach all control volumes and cell faces are specified in a one-dimensional manner. The information regarding neighbouring cells and surrounding faces related to each control volume must be stored in advance. By this method there is no need to make coordinate transformation. Another merit is that the control volume is not restricted to be rectangular and can be a polygon of arbitrary geometry.

After integration the volume integrals of the convection and diffusion terms are transformed into surface integrals *via* applying the divergence theorem of Gauss. The convective and diffusive

DOI: 10.1002/fld

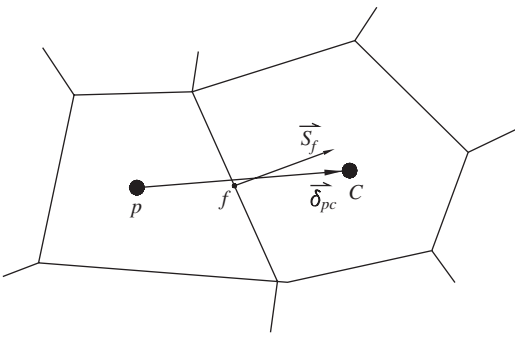

Figure 2. Illustration of a typical control volume and a neighbouring cell.

momentum fluxes through the surface of the control volume can be expressed as

$$F^{\mathrm{c}} = \sum_f (\mathbf{V} \bullet \mathbf{s})_f \phi_f \tag{3}$$

$$F^{\mathrm{d}} = \sum_f (v \nabla \phi \bullet \mathbf{s})_f \tag{4}$$

where subscripts f denote the value at a face of the control volume, ϕ represents a velocity component, $\mathbf{V}$ is the velocity vector, $\mathbf{s}_f$ the surface vector of the considered face, and v the kinematic viscosity. The summation is taken over all the surrounding faces.

In the convective flux the face value ϕ_f is approximated by the central difference in a deferred correction manner. For the diffusive flux further discretization is needed. A variety of approximations were proposed in the literature. But, as shown by Tsui and Pan [24], these expressions are equivalent to the following form

$$F_f^{\mathrm{d}} = \frac{v_f s_f^2}{\boldsymbol{\delta}_{PC} \bullet \mathbf{s}_f} (\phi_C - \phi_P) + v_f \overline{\nabla \phi}_f \bullet \left(\mathbf{s}_f - \frac{s_f^2}{\boldsymbol{\delta}_{PC} \bullet \mathbf{s}_f} \boldsymbol{\delta}_{PC} \right) \tag{5}$$

where, see Figure 2, the subscripts P and C denote the principal node and a neighbouring node sharing the common face f, and $\boldsymbol{\delta}_{PC}$ is the vector connecting these two nodal points. The gradient on the face $\overline{\nabla \phi}_f$ is obtained *via* interpolation from the gradients at the two nodes P and C. For grids with the surface vector $\mathbf{s}_f$ in the same direction as $\boldsymbol{\delta}_{PC}$, such as the rectangular grid used in the present study, the second term on the right-hand side vanishes because the two terms in the parentheses become identical. The remaining first term simply represents a central difference approximation.

All variables are placed on the centroid of each control volume. This collocation arrangement may lead to decoupling between the velocity and the pressure fields unless special treatments are taken. To avoid solution oscillation the momentum interpolation method [25] is employed to calculate the mass flux through each face.

DOI: 10.1002/fld

Following the SIMPLE algorithm [26], a pressure-correction equation can be obtained by invoking the continuity constraint as

$$\sum_f (\Gamma \nabla p' \bullet \mathbf{s})_f = -\sum_f \dot{m}_f^* \tag{6}$$

where p' is the pressure correction, $\dot{m}_f^*$ is the mass flux obtained in the momentum predictor step, and Γ is a diffusion-like coefficient for p'. The term on the left-hand side represents the sum of diffusive fluxes over all the surrounding faces and that on the right-hand side the mass accumulated in the considered control volume. By using the approximation given in Equation (5) for the diffusive fluxes for p' a pressure-correction equation is yielded

$$A_P p'_P = \sum_C A_C p'_C + S_{p1} + S_{p2} \tag{7}$$

where

$$S_{p1} = -\sum_f m_f^* \tag{8a}$$

$$S_{p2} = \sum_f \Gamma_f \overline{\nabla p'_f} \bullet \left(\mathbf{s}_f - \frac{s_f^2}{\boldsymbol{\delta}_{PC} \bullet \mathbf{s}_f} \boldsymbol{\delta}_{PC} \right) \tag{8b}$$

It is emphasized here that for rectangular grids the term S_{p2} and the second part in the diffusive flux simply disappear, resulting in the same difference forms given by Patankar [26].

4. RESULTS AND DISCUSSION

Rectangular grids were employed in the calculation. The grid density has been carefully selected to ensure real flow physics not being shadowed by discretization errors. In the vertical plane (x–z plane) the number of nodes in the upstream channel is 30×12 and that in the expanded channel is 80×36. The grid lines are distributed in a non-uniform manner with denser grids in the regions near the walls and the expansion. The grid spacings in the x- and z-directions are within the ranges 0.25–1.27 and 0.05–0.14, respectively. It will be seen later from the bifurcation diagram given in Figure 8 that with this grid the predicted reattachment lengths for the recirculating flows in the three-dimensional channel with an aspect ratio 8 are in close agreement with those obtained in two-dimensional calculations using a grid with 20 000 nodal points. The coordinate in the spanwise direction is designated as y-axis. The node number in this direction depends on the aspect ratio. For aspect ratios higher than 2.3 the node number is 79. It gradually reduces to 12 for aspect ratios less than 0.33. The grid size Δy ranges from 0.05 to 0.4.

In order to assess the mathematical model, calculations have been conducted for Reynolds numbers $Re = 34.7$, 80, and 186.7, which are referred to as $Re = 26$, 60, and 140 in the study of Fearn *et al*. [7]. The cause of the difference is due to the different definitions used for the Reynolds number. For aspect ratio 8, as adopted in both computations and experiments, the effect of the side wall on the flow in the centre x–z plane can be ignored, especially for the two low Reynolds numbers. Comparison of axial velocity between predictions and measurements at a number of

DOI: 10.1002/fld

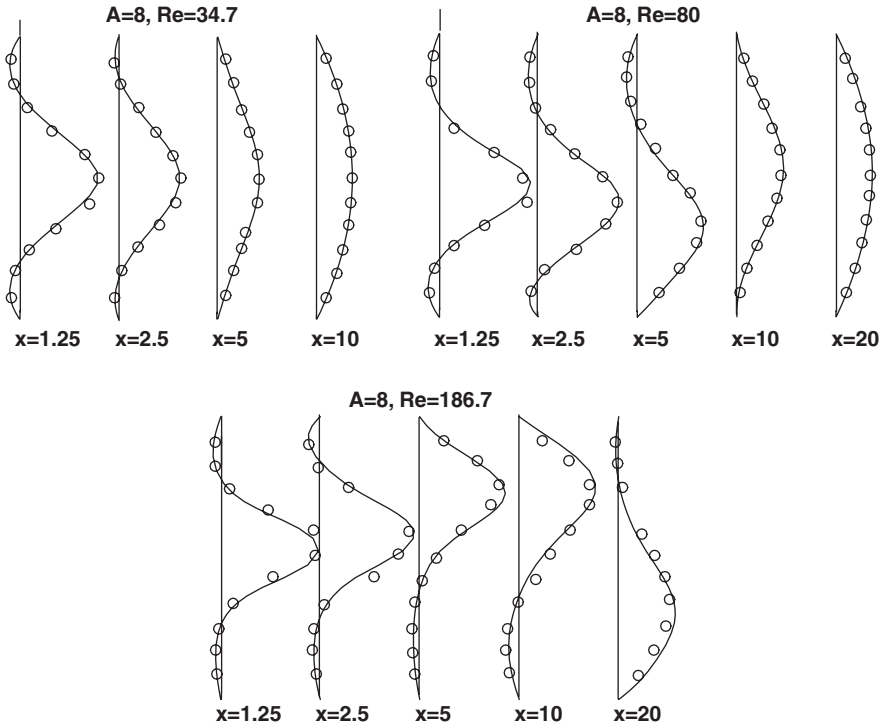

Figure 3. Comparison of axial velocity with measurements.

stations in the centre plane is made in Figure 3. At the sub-critical Reynolds number of 34.7 the flow is symmetric. By increasing the Reynolds number to 80 the flow becomes asymmetric, with two recirculation regions of different sizes on the top and bottom walls. Further increase of the Reynolds number to 186.7 results in a third recirculation zone formed on the same side of the weaker one of the above two, which is visible at station $x = 20h$. Good agreement between the two set of data can be seen, especially for the two low Reynolds numbers. This validates our mathematical method which is used in the following computations.

The sizes of the recirculation zones, represented by reattachment lengths, for aspect ratios $A = \frac{1}{3}, 1, 4$ and 8 are presented in Figures 4–7. It is evident that the flow is stabilized by the side wall as the channel becomes narrow. For aspect ratio $\frac{1}{3}$ the flow remains symmetric for all Reynolds numbers under consideration. As the aspect ratio is increased to 1, a visible breaking of the symmetric pattern occurs at a Reynolds number of around 92. The reattachment length of the larger recirculation region x_1 continues to increase with the increasing Reynolds number while that of the smaller one x_2 decreases first, and then approaches a constant value of about $4.5h$. By increasing the aspect ratio to 4 the bifurcation point shifts to a lower Reynolds number of about 61. The variation of the two reattachment lengths with respect to the Reynolds number behaves in a similar manner to the case of aspect ratio 1. However, as the Reynolds number becomes larger than about 125, a third recirculation region is found on the side of the smaller of the two main recirculation zones. Both the main recirculating flows reduce in size while the

DOI: 10.1002/fld

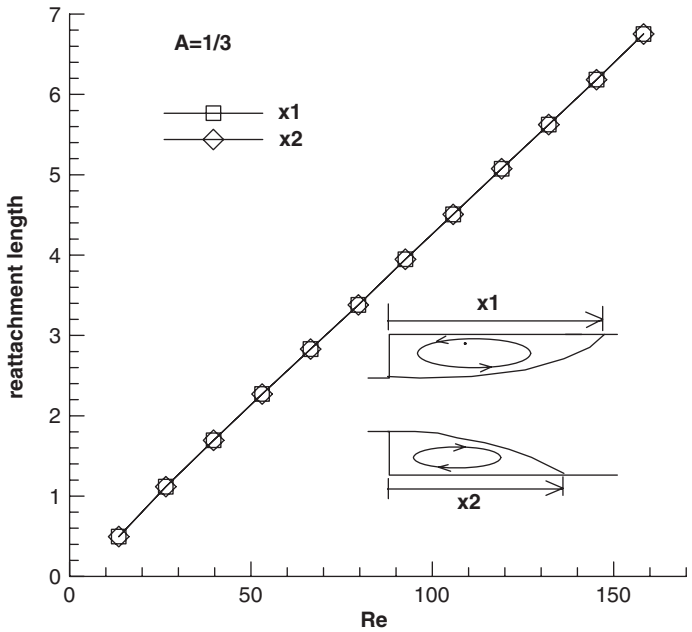

Figure 4. Variation of reattachment length with Reynolds number for aspect ratio $A = \frac{1}{3}$.

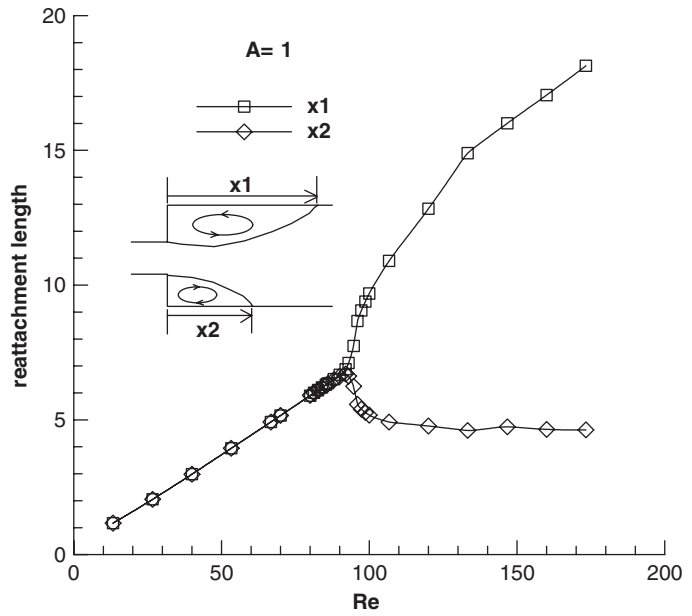

Figure 5. Variation of reattachment length with Reynolds number for aspect ratio $A = 1$.

DOI: 10.1002/fld

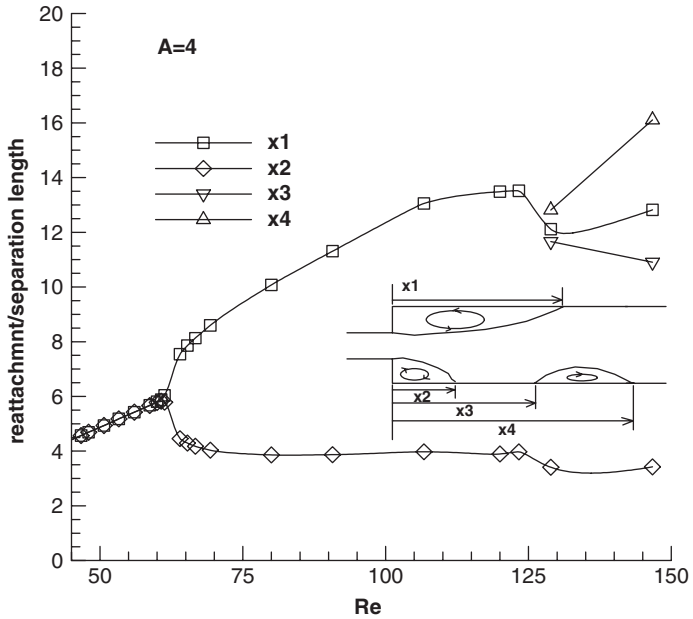

Figure 6. Variation of reattachment/separation length with Reynolds number for aspect ratio $A = 4$.

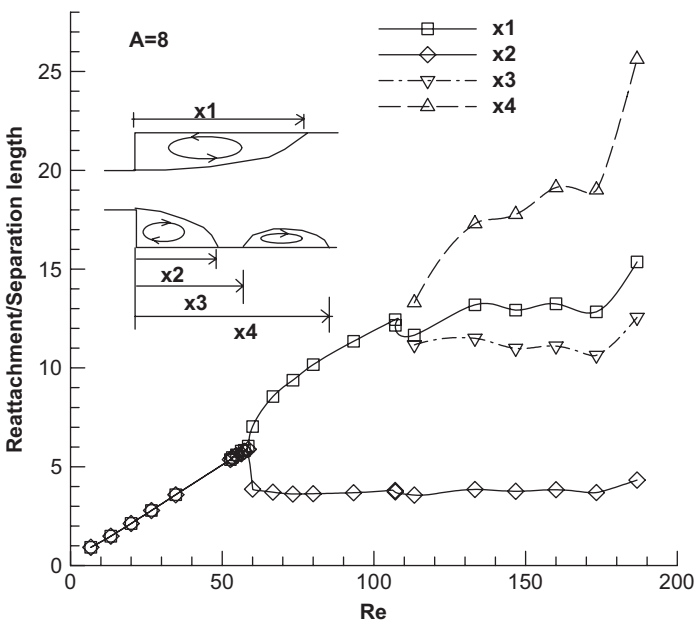

Figure 7. Variation of reattachment/separation length with Reynolds number for aspect ratio $A = 8$.

DOI: 10.1002/fld

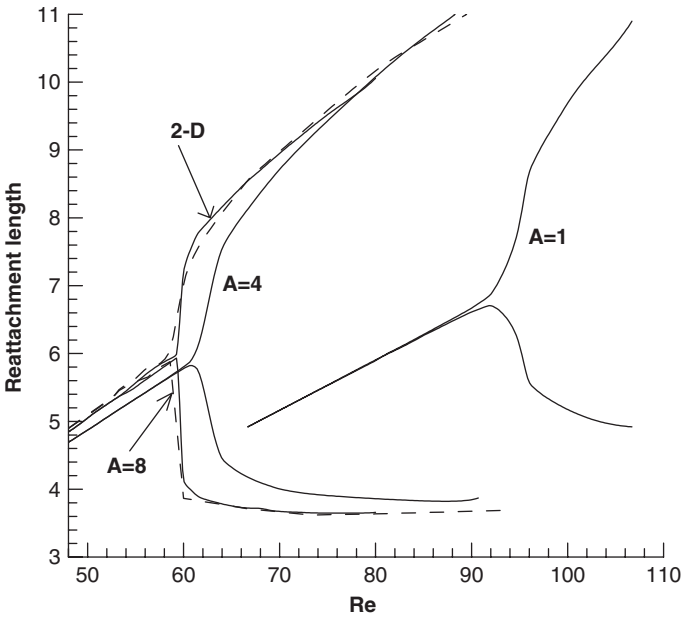

Figure 8. Variation of reattachment length with Reynolds number for aspect ratios $A = 1$, 4, and 8, and for two-dimensional channel.

third one appears. Further increase of the aspect ratio to 8 reduces the critical Reynolds number slightly to about 58.5 and results in a lower Reynolds number of around 110 for the appearance of the third recirculation zone. It is noted from the above figures that if the flow remains symmetric, the reattachment lengths vary linearly with the Reynolds number. The bifurcation diagrams in the region near the critical Reynolds number for the three high aspect ratio cases are reproduced in Figure 8. Also included is a two-dimensional calculated result. It is obvious that in comparison with the two-dimensional predictions, there still exists a considerable difference for aspect ratio 4. For aspect ratio 8 the side-wall effect can be neglected and the flow on the centre plane can be regarded as two-dimensional. As mentioned before, a grid with 20 000 nodes was employed in the two-dimensional calculation, which is much finer than the one used in the x–z plane of the three-dimensional calculation. This result helps justify the grid used in the three-dimensional computation.

The effect of aspect ratio is further demonstrated in Figures 9 and 10 for Reynolds numbers fixed at 80 and 133, respectively. For $Re = 80$ bifurcation takes place at an aspect ratio 1.25. For aspect ratio greater than 5 the asymmetric pattern remains almost unchanged, with a larger recirculation region of size $10h$ and a smaller one of size $3.7h$, implying that the flow becomes two-dimensional. At the high Reynolds number of 133 the critical aspect ratio is reduced to around 0.5. For this case a third recirculating flow is found as aspect ratio becomes greater than 3. At sufficiently high aspect ratios the smaller main recirculating flow remains at a size of about $4h$. But the larger one reduces its reattachment length first, followed by an increase. The continuous change of this reattachment point, together with the changing position of the third recirculation region, indicates that the influence of the side wall cannot be ignored even for aspect ratio greater than 8.

DOI: 10.1002/fld

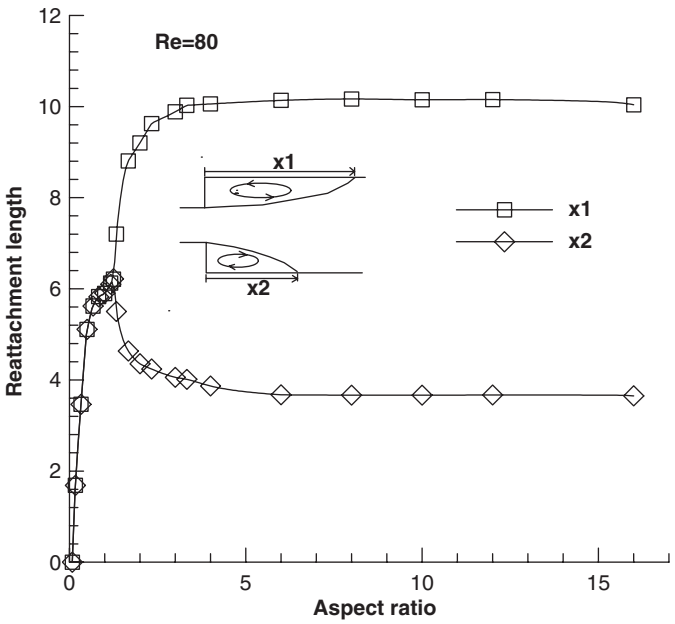

Figure 9. Variation of reattachment length with aspect ratio for $Re = 80$.

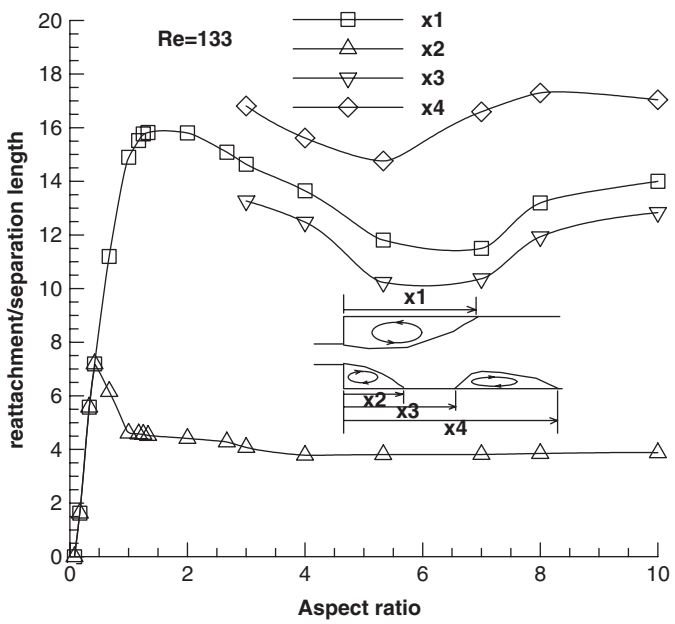

Figure 10. Variation of reattachment/separation length with aspect ratio for $Re = 133$.

DOI: 10.1002/fld

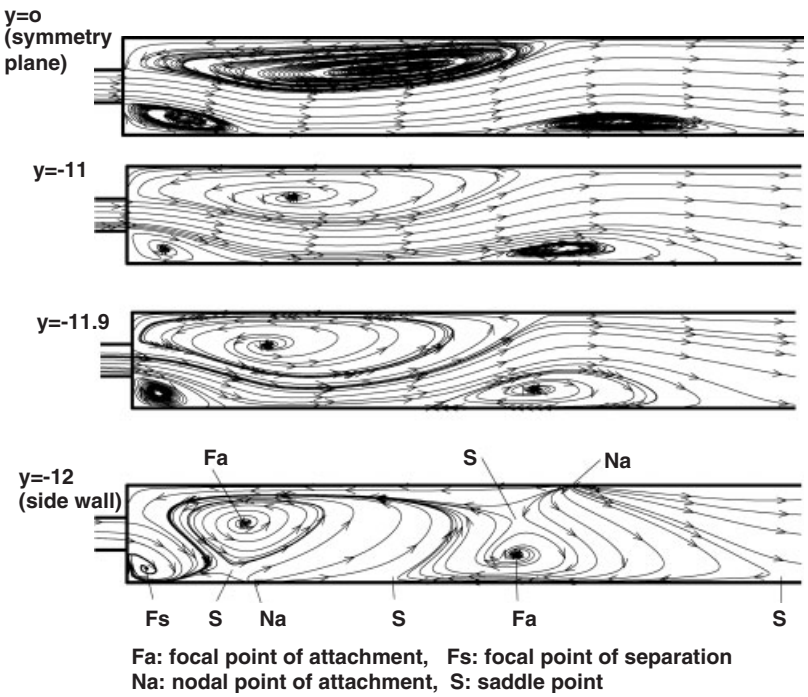

Figure 11. Streamlines at different spanwise stations for $A = 8$ and $Re = 160$.

The flow structure is illustrated on various x–z planes at a number of spanwise locations in Figures 11–13 for aspect ratios 8, 4, and 1, respectively. At $Re = 160$ for aspect ratio 8 a triple-vortex pattern prevails throughout the spanwise direction, as seen in Figure 11. In the spanwise direction up to $y = -11h$ the three vortices remain nearly invariant in size. In the region near the side wall the large vortex behind the upper step and the third vortex expand their sizes in the vertical direction, as evident at $y = -11.9h$. Limiting streamlines (or skin friction lines) have been widely used to study three-dimensional separated flows. In topology theory singular points occur at points where skin friction becomes zero. Singular points are classified into nodes and saddles. Nodes can be further divided into nodal points and focal points [27, 28]. The limiting lines on the side wall ($y = -12h$) show that either the large vortex near the upper step or the third vortex on the lower wall degenerates into a focal point of attachment (Fa), which acts as a source of limiting streamlines that draws fluid from the core region and spays over the wall surface. The small vortex behind the lower step is transformed into a focal point of separation (Fs) which behaves like a sink where the fluid collected from the wall surface will eventually be carried away in the spanwise direction. This indicates that a particle originally located near this point will be transported towards the channel core. The attachment point of the large main vortex on the upper wall becomes a nodal point of attachment (Na). There is a saddle point (S) between this node and the focus of attachment of the third vortex. The separation and reattachments points of the third vortex on the lower wall are transformed into saddle points. At the region near the reattachment point of the small vortex behind the lower step a saddle point and a nodal point of attachment are

DOI: 10.1002/fld

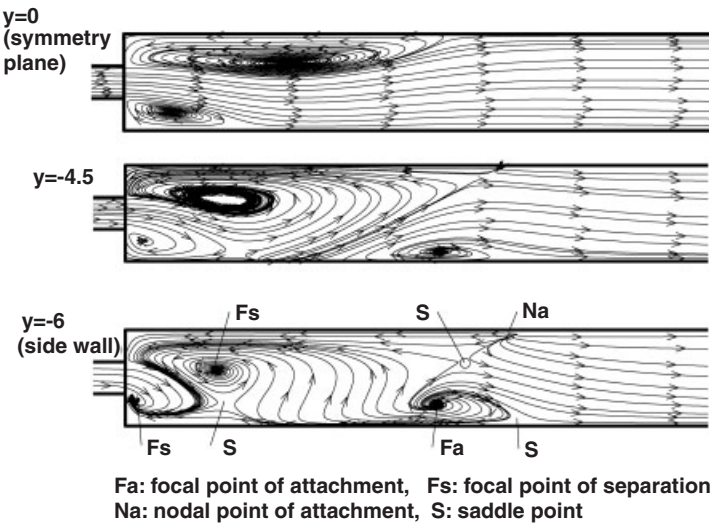

Figure 12. Streamlines at different spanwise stations for $A = 4$ and $Re = 80$.

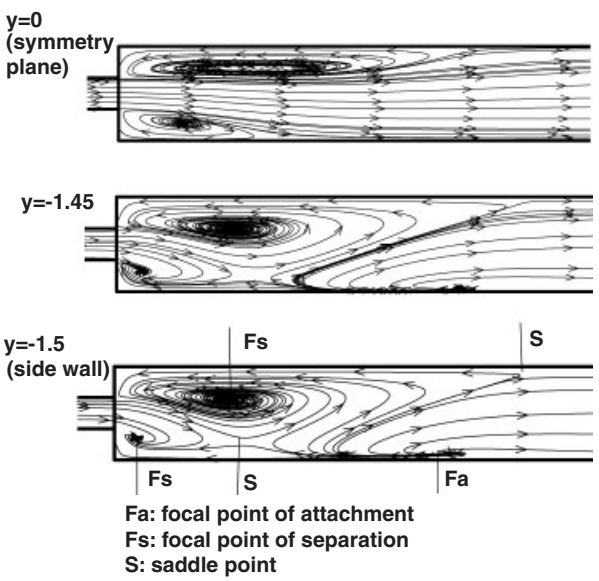

Figure 13. Streamlines at different spanwise stations for $A = 1$ and $Re = 160$.

found. Totally, there are five nodes (three focal points and two nodal points) and four saddles on the side wall.

For aspect ratio 4 with $Re = 80$ (see Figure 12) only two vortices are seen in the channel core. However, a third vortex is formed near the side wall, which was also observed by Chiang *et al*. [21].

DOI: 10.1002/fld

The limiting streamlines show that the large vortex near the upper step is not transformed into a focal point of attachment, but a focal point of separation. One nodal point as well as one saddle point on the lower wall seen in the previous figure disappears from the plot. The flow topology is modified by directing the limiting streamlines from the focal point of attachment at the downstream location directly towards the focal point of separation behind the upper step. The number of nodes is reduced to 4 and that of saddles to 3.

For the case with aspect ratio 1 and $Re = 160$ (see Figure 13) the double-vortex pattern is seen in the entire spanwise direction. However, there still exists a focal point of attachment which is degenerated from the third vortex in the above cases. This focal point is shifted to the bottom wall. The saddle point transformed from the reattachment point of the third vortex seen in the above figure does not exist any longer. In the meanwhile the saddle point above this focus moves to the upper wall and the nodal point there is eliminated. Thus, only three nodes and two saddles are found. It can be concluded from the above results that if a non-symmetric flow pattern prevails, the total number of nodes $\sum_N$ and the total number of saddles $\sum_S$ on the side wall are related as

$$\sum_N - \sum_S = 1 \tag{9}$$

As reported by Fearn *et al*. [7], due to the unavoidable imperfections in the experimental apparatus, perfectly symmetric flow patterns could not be obtained. As a result, the bifurcation diagram broke into two separate branches and the critical Reynolds number could not be determined in their experiments. Hawa and Rusak [9] and Mizushima and Shiotani [10] used nonlinear stability analysis to verify that a gradual evolution from symmetric states to asymmetric states occurs in

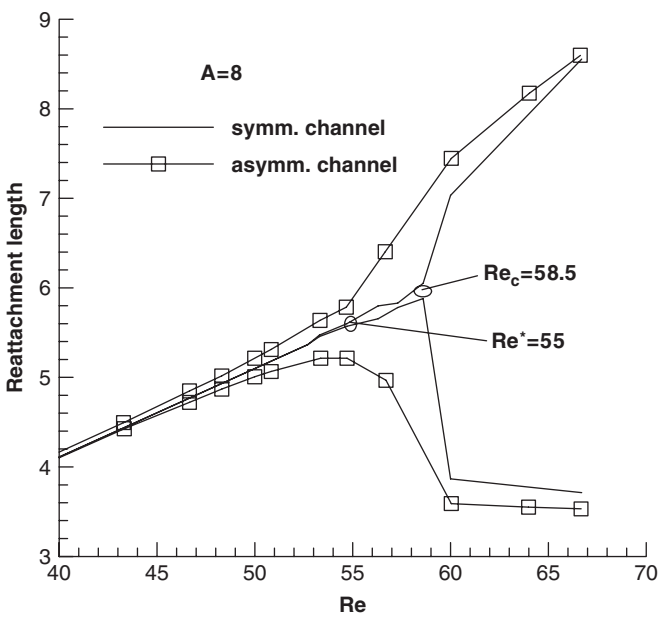

Figure 14. Comparison of reattachment length between the symmetric and the slightly asymmetric channel flows for aspect ratio $A = 8$.

DOI: 10.1002/fld

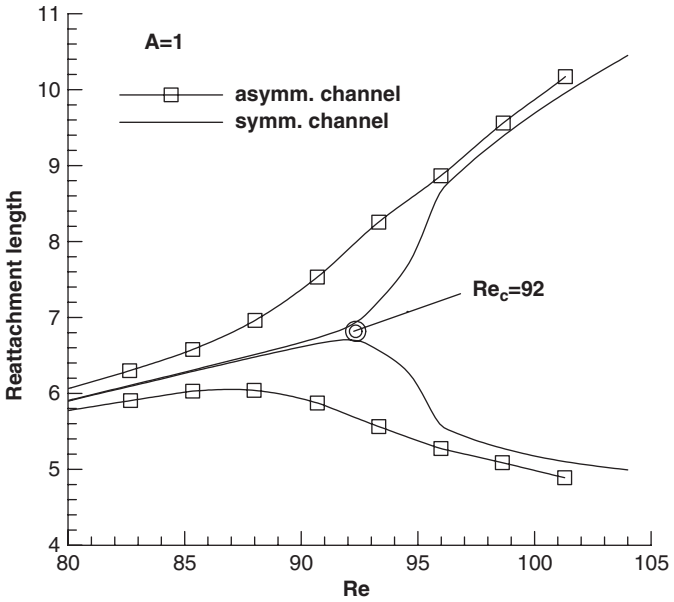

Figure 15. Comparison of reattachment length between the symmetric and the slightly asymmetric channel flows for aspect ratio $A = 1$.

a primary branch. Following Fearn *et al*., the imperfectness of the system is created by using a slightly non-symmetric geometry. The computations conducted in the following are based on the expanded channel shown in Figure 1 with the upper wall being shifted upwards by a small extent of $0.05h$. The phenomenon of the smooth transition from the symmetric state to the asymmetric state is demonstrated in Figures 14 and 15 for aspect ratios 8 and 1. Away from the bifurcation region the solution for the non-symmetric channel approaches that for the symmetric channel.

An interesting point regarding the critical Reynolds number needs to be addressed in the following. The critical Reynolds number for the symmetric channel flow Re_c is marked in the bifurcation diagrams in Figures 14 and 15. It can be detected that before this critical point is reached, a slight deviation between the two reattachment lengths had already been in progress. A similar phenomenon was also addressed by Neofytou and Drikakis [13] in their non-Newtonian flow calculations and could be identified in the bifurcation diagrams in the three-dimensional study of Schreck and Schafer [20]. For the low aspect ratio 1 this deviation varies in a more gradual fashion. For aspect ratio 8 a rather significant deviation point at around $Re^* = 55$ can be identified. It is seen from Table I that the present critical value of 58.5 is comparable to the value of 58.7 given by De Zilwa *et al*. [18] and that in the range 57–58 reported by Battaglia *et al*. [16]. All these results are obtained using numerical simulations, which, in general, are higher than those determined by the bifurcation theory. But the value $Re^* = 55$ is close to the theoretical one, say, 53.9 reported by Fearn *et al*. [7]. This indicates the difficulty to exactly pinpoint the bifurcation point by both the numerical simulations and the experiments; this point would rely on how to define asymmetric flow.

DOI: 10.1002/fld

5. CONCLUSIONS

A mathematical method incorporating unstructured grids has been used to examine the side wall effect on the bifurcating flow in a channel with a symmetric sudden expansion. A summary of the main results is given as follows:

(1) For aspect ratio 8 the breaking of symmetric flow occurs at a Reynolds number of 58.5. By reducing the aspect ratio to 4 and 1 the critical Reynolds number is increased to 61 and 92. By further decreasing the aspect ratio to $\frac{1}{3}$ the flow remains symmetric for all Reynolds numbers considered. This result implies that the appearance of the side wall by reducing the aspect ratio has a stabilizing effect on the flow.
(2) For high aspect ratios together with high Reynolds numbers a third recirculation zone can be seen in all the planes throughout the spanwise direction. When either the aspect ratio or the Reynolds number is decreased, the third recirculation zone appears only in the region near the side wall. Each of the number of nodes and the number of saddles on the side wall is reduced by 1. Further decreasing the aspect ratio or the Reynolds number results in complete elimination of the third recirculation zone from the channel. As a consequence, the total numbers of nodes and saddles are further reduced by 1 individually. It can be concluded that the total node number is greater than the total saddle number by 1 for the asymmetric flows.
(3) The critical Reynolds number of 58.5 obtained for aspect ratio 8 is somewhat higher than the theoretical value obtained from two-dimensional bifurcation theory. However, slightly asymmetric solutions can be traced to a lower Reynolds number of 55 which is close to the theoretical one. Therefore, the determination of the bifurcation point would depend upon how to distinguish between symmetric and asymmetric flows in numerical simulations.
(4) It is confirmed that an imperfection in the flow system would result in smooth transition from the symmetric state to the asymmetric state.

ACKNOWLEDGEMENT

This work was supported by National Science Council of Republic of China under contract numbers NSC-91-2212-E-009-051 and NSC-93-2212-E-009-012.

REFERENCES

1. Durst F, Melling A, Whitelaw JH. Low Reynolds number flow over a plane symmetric sudden expansion. *Journal of Fluid Mechanics* 1974; **64**:111–128.
2. Willie R, Fernholz H. Report on the first European Mechanics Colloquium, on the Coanda effect. *Journal of Fluid Mechanics* 1965; **23**:801–819.
3. Sobey IJ, Drazin PG. Bifurcations of two-dimensional channel flows. *Journal of Fluid Mechanics* 1986; **171**: 263–287.
4. Cherdron W, Durst F, Whitelaw JH. Asymmetric flows and instabilities in symmetry ducts with sudden expansions. *Journal of Fluid Mechanics* 1978; **84**:13–31.
5. Tsui Y-Y, Wang C-K. Calculation of laminar separated flow in symmetric two-dimensional diffusers. *Journal of Fluids Engineering* (ASME) 1995; **117**:612–616.
6. Tsui Y-Y, Shu S-J. Effects of buoyancy and orientation on the flow in a duct preceded with a double-step expansion. *International Journal of Heat and Mass Transfer* 1998; **41**:2687–2695.

DOI: 10.1002/fld

7. Fearn RM, Mullin T, Cliffe KA. Nonlinear flow phenomena in a symmetric sudden expansion. *Journal of Fluid Mechanics* 1990; **211**:595–608.
8. Shapira M, Degani D, Weihs D. Stability and existence of multiple solutions for viscous flow in suddenly enlarged channels. *Computers and Fluids* 1990; **18**:239–258.
9. Hawa T, Rusak Z. Viscous flow in a slightly asymmetric channel with a sudden expansion. *Physics of Fluids* 2000; **12**:2257–2267.
10. Mizushima J, Shiotani Y. Structural instability of the bifurcation diagram for two-dimensional flow in a channel with a sudden expansion. *Journal of Fluid Mechanics* 2000; **420**:131–145.
11. Durst F, Pereira JCF, Tropea C. The plane symmetric sudden-expansion flow at low Reynolds numbers. *Journal of Fluid Mechanics* 1993; **248**:567–581.
12. Mizushima J, Okamoto H, Yamaguchi H. Stability of flow in a channel with a suddenly expanded part. *Physics of Fluids* 1996; **8**:2933–2942.
13. Neofytou P, Drikakis D. Non-Newtonian flow instability in a channel with a sudden expansion. *Journal of Non-Newtonian Fluid Mechanics* 2003; **111**:127–150.
14. Alleborn N, Nandakumar K, Raszillier H, Durst F. Further contributions on the two-dimensional flow in a sudden expansion. *Journal of Fluid Mechanics* 1997; **330**:69–188.
15. Rusak Z, Hawa T. A weakly nonlinear analysis of the dynamics of a viscous flow in a symmetric channel with a sudden expansion. *Physics of Fluids* 1999; **11**:3629–3636.
16. Battaglia F, Tavener SJ, Kulkarni AK, Merkle CL. Bifurcation of low Reynolds number flows in symmetric channels. *AIAA Journal* 1997; **35**:99–105.
17. Drikakis D. Bifurcation phenomena in incompressible sudden expansion flows. *Physics of Fluids* 1997; **9**:76–87.
18. De Zilwa SRN, Khezzar L, Whitelaw JH. Flows through plane sudden-expansions. *International Journal for Numerical Methods in Fluids* 2000; **32**:313–329.
19. Foumeny EA, Ingham DB, Walker AJ. Bifurcations of incompressible flow through plane symmetric channel expansions. *Computers and Fluids* 1996; **25**:335–351.
20. Schreck E, Schafer M. Numerical study of bifurcation in three-dimensional sudden channel expansions. *Computers and Fluids* 2000; **29**:583–593.
21. Chiang TP, Sheu TWH, Wang SK. Side wall effects on the structure of laminar flow over a plane-symmetric sudden expansion. *Computers and Fluids* 2000; **29**:467–492.
22. Chiang TP, Sheu TWH, Hwang RR, Sau A. Spanwise bifurcation in plane-symmetric sudden-expansion flows. *Physical Review E* 2001; **65**:016306.
23. Biswas B, Breuer M, Durst F. Backward-facing step flows for various expansion ratios at low and moderate Reynolds numbers. *Journal of Fluids Engineering* (ASME) 2004; **126**:362–374.
24. Tsui Y-Y, Pan Y-F. A pressure-correction method for incompressible flow using unstructured meshes. *Numerical Heat Transfer B* 2006; **49**:43–65.
25. Rhie CM, Chow WL. Numerical study of the turbulent flow past an airfoil with trailing edge separation. *AIAA Journal* 1983; **21**:1525–1532.
26. Patankar SV. *Numerical Heat Transfer and Fluid Flow*. Hemisphere Publishing Corporation: New York, 1980.
27. Hunt JCR, Abell CJ, Peterka JA, Woo H. Kinematical studies of the flows around free or surface-mounted obstacles; applying topology to flow visualization. *Journal of Fluid Mechanics* 1978; **86**:179–200.
28. Tobak M, Peake DJ. Topology of three-dimensional separated flows. *Annual Review of Fluid Mechanics* 1982; **14**:61–85.

DOI: 10.1002/fld